Available online at www.sciencedirect.com
SCIENCE DIRECT®
International Journal of Solids and Structures 42 (2005) 337–351
INTERNATIONAL JOURNAL OF SOLIDS and STRUCTURES
www.elsevier.com/locate/ijsolstr

Micromechanical modelling of cyclic plasticity incorporating damage

D. Steglich [a,*], A. Pirondi [b], N. Bonora [c], W. Brocks [a]

[a] Institute for Materials Research, GKSS Research Centre, Max-Planck-Str. 1, D-21502 Geesthacht, Germany
[b] Department of Industrial Engineering, University of Parma, I-43100 Parma, Italy
[c] DIMSAT, University of Cassino, I-03043 Cassino, Italy

Received 26 April 2004; received in revised form 14 June 2004
Available online 26 August 2004

Abstract

In this paper a numerical investigation on the possibility to simulate and predict cyclic plastic response incorporating damage has been performed. To this purpose, unit cell and continuum approaches based on porous metal plasticity and continuum damage mechanics (CDM) have been considered. In particular, the porous metal plasticity model of Leblond, Perrin and Devaux (LPD model) and the CDM model developed by Pirondi and Bonora were used. Finite element (FE) simulations were performed for each approach with different degrees of triaxiality and the results are analyzed and compared.

Keywords: Cyclic plasticity; Cell models; Porous plasticity models; Continuum damage mechanics

1. Introduction

Nowadays, micromechanics is a recognized powerful methodology for the investigation and prediction of materials behavior at the meso/macroscale using characteristics of the microstructure through the analysis of periodic representative volume elements (RVEs, meso-elements), see e.g. Nemat-Nasser and Hori (1993) and Aboudi (1989). For this purpose, unit cells have to be defined in order to capture the microstructural features to be described. One of the major advantages offered by micromechanical modelling is the possibility to incorporate damage processes and to follow the associated progressive degradation of the RVE by monitoring the overall properties. In the literature, micromechanics has been successfully used

* Corresponding author. Tel.: +49 4152 872543; fax: +49 4152 872595.
E-mail address: dirk.steglich@gkss.de (D. Steglich).

0020-7683/$ - see front matter © 2004 Elsevier Ltd. All rights reserved.
doi:10.1016/j.ijsolstr.2004.06.041

Nomenclature

b	isotropic hardening exponent
d_{ij}	Eulerian strain rate tensor
$h^{(\alpha)}$	internal variables for isotropic hardening
q	stress deviator related part of the yield function
$q_1; q_2; q_3$	parameters of the GTN and LPD models
p	hydrostatic stress related part of the yield function
C	kinematic hardening modulus
D	damage variable in CDM
D_0	initial damage in CDM
D_{cr}	critical damage in CDM
E_0	Young's modulus of undamaged material
E	effective (damaged) Young's modulus
E_i	mesoscopic strain ($i = 1, 2, 3$)
E_{eq}	mesoscopic equivalent strain
$H\langle\rangle$	step function
f	void volume fraction
f_{c}	critical void volume fraction
f^*	damage variable in GTN and LPD
R	current radius of the yield surface
R_0	initial yield stress (zero plastic strain)
R_∞	saturated radius of the yield surface
T	stress triaxiality
x_{ij}	backstress tensor
x'_{ij}	backstress tensor deviator
α	damage exponent
ε_{ij}	strain tensor
$\varepsilon_{ij}^{\mathrm{el}}$	elastic strain tensor
$\varepsilon_{ij}^{\mathrm{pl}}$	plastic strain tensor
$\varepsilon_{\mathrm{cr}}$	theoretical failure strain under uniaxial state of stress ($T = 0.333$)
$\varepsilon_{\mathrm{th}}$	damage threshold strain (uniaxial)
$\varepsilon_{\mathrm{eq}}^{\mathrm{pl}}$	accumulated equivalent plastic strain
γ	kinematic hardening exponent
κ	damage acceleration parameter
λ	plastic multiplier
σ_{eq}	equivalent von Mises stress
σ_{ij}	Cauchy stress tensor
σ_m	mean stress
ν	Poisson's ratio
Φ	yield function
Σ_i	mesoscopic stress ($i = 1, 2, 3$)
Σ_m	mesoscopic mean stress
Σ_{eq}	mesoscopic equivalent stress

to predict overall behavior of composites at the macroscale as well as damage evolution in more traditional materials such as metals. In most of the cases the modelling has been focused in predicting materials constitutive response under monotonic loading only.

However, engineering components and structures may be subjected to loading conditions, which can force the material to undergo cyclic plastic flow. The occurrence of plastic deformation and accumulation with cycles is a cause of damage development that, sooner or later, will lead the material to fail. Damage is related to the irreversible processes that occur in the materials microstructure, therefore its presence affects the material constitutive response at meso/macro scale. Examples for this particular loading case are earthquake loadings, overloads and the reeling of pipelines. Under cyclic plastic loading, irreversible microstructural changes take places, in order of increasing strain amplitude, in the following forms: persistent slip bands, rearrangement of dislocation systems into cell structures, and void nucleation and growth at the secondary phase inclusions (Klesnil and Lukas, 1980; Polak, 1991). The latter mechanism is peculiar of high strain amplitudes, for which very short lives are usually expected.

Void nucleation and growth has been firstly recognized as the key micromechanism of rupture for ductile metals by Mc Clintock (1968) and Rice and Tracey (1969) who also proposed a failure criterion based on the growth of cavities. Since then, many models and criteria have been proposed in the literature. Today, these approaches can be sorted in three main classes: (i) abrupt failure criteria, (ii) porous metal plasticity, and (iii) continuum damage mechanics (CDM). The major feature of these approaches based on continuum mechanics is, in principle, the transferability from specimen to structure since model parameters should be geometry-independent. In the first group, ductile failure is predicted when a micromechanical variable, for instance the cavity growth rate (Rice and Tracey, 1969), reaches a critical value characteristic of the material. In the second group, the damage effects are accounted for into the plastic potential by a softening term, which is usually related to volume fraction of voids in the material. This internal variable induces a progressive shrinkage of the yield surface until failure occurs due to loss of stress carrying capability. Gurson (1977) derived a void evolution law from the analytical study of a single isolated cavity in an elastic-perfectly plastic matrix. Needleman and Rice (1978) extended the Gurson model in order to account for the effects associated to secondary particles nucleating voids. Tvergaard and Needleman (1984) further modified the Gurson model in order to take into account the acceleration of the failure process induced by voids coalescence (GTN model). A porous metal plasticity model based on thermodynamical principles has been developed by Rousselier (1987).

The CDM approach instead, initially proposed by Lemaitre (1985), considers the effects associated to a given damage condition through the definition of a thermodynamic state variable. In this framework, the set of constitutive equations for the damaged material is derived under the assumption of the existence of a damage potential uncoupled from that for plasticity. Damage affects not only the material's yield function but also reduces the stiffness through the definition of the effective stress. Many authors modified the Lemaitre linear damage formulation in order to fit experimental damage measurements relative to different classes of metals, see for example Chandrakanth and Pandey (1993). Recently, Bonora (1997) proposed a modified nonlinear CDM model that overcomes some of the disadvantages showed by other formulations, such as large number of damage parameters, the lack of transferability of damage parameters to multi-axial stress and the inadequacy of describing damage evolution for different classes of metals.

So far, very little attention has been given to the possibility to investigate cyclic plasticity by means of micromechanics incorporating damage. As far as the groups of models discussed above is concerned, Leblond et al. (1995) as well as Besson and Guillemer-Neel (2003) introduced nonlinear kinematic hardening into the GTN model while Pirondi and Bonora (2003) extended the nonlinear CDM model (Bonora, 1997) to tension–compression loading.

In this paper, numerical investigations on the possibility to simulate and predict cyclic plastic response of metals incorporating damage has been performed. To this purpose, both the unit cell model and the continuum RVE approaches have been analyzed and the results have been compared. In Section 2, the

constitutive equations of rate-independent plasticity are briefly reviewed. In Section 3, the unit cell model, LPD and CDM formulations for the description of cyclic plastic loading of ductile metals in Section 3 are summarized. Details on the material properties considered in this study and FE modelling are given. Finally, in Section 5, the results obtained with the three formulations are presented and discussed.

2. Rate-independent plasticity

Inelastic deformations are described in the framework of the classical theory of rate-independent plasticity. The yield function has the general form

$$\Phi(q,p,h^{(\alpha)}) \leqslant 0; \quad q=\sqrt{\frac{3}{2}s'_{ij}s'_{ij}}, \quad p=-\frac{1}{3}s_{kk}, \tag{1}$$

s'_{ij} denoting the deviatoric part of the tensor s_{ij}. The dependence of Φ on p vanishes for incompressible plastic deformations, but appears in pressure-dependent plasticity. The difference between Cauchy stresses, σ_{ij}, and back stresses, x_{ij}, for kinematic hardening,

$$s_{ij}=\sigma_{ij}-x_{ij}, \tag{2}$$

is used. The scalar quantities $h^{(\alpha)}$ denote internal variables for isotropic hardening or softening. The (symmetric) strain rate deformation tensor is decomposed in an elastic and a plastic contribution,

$$d_{ij}=d^{\mathrm{el}}_{ij}+d^{\mathrm{pl}}_{ij}, \tag{3}$$

which is equivalent to the multiplicative decomposition of the respective displacement gradients for small elastic strains. Hooke's law is assumed for elastic deformation rates and Jaumann stress rates according to the Hughes and Winget (1980) approach

$$\overset{\nabla}{\sigma}_{ij}=C_{ijkl}d^{\mathrm{el}}_{ij}=C_{ijkl}(d_{ij}-d^{\mathrm{pl}}_{ij}). \tag{4}$$

An associated flow (or normality) rule

$$d^{\mathrm{pl}}_{ij}=\dot{\lambda}\frac{\partial\Phi}{\partial\sigma_{ij}}=\dot{\lambda}\left(\frac{\partial\Phi}{\partial q}n_{ij}-\frac{1}{3}\frac{\partial\Phi}{\partial p}\delta_{ij}\right)=\dot{e}_q n_{ij}+\frac{1}{3}\dot{e}_p\delta_{ij}; \quad \text{with } n_{ij}=\dot{\lambda}\frac{3s_{ij}}{2q} \tag{5}$$

is postulated for the plastic deformation rates. The two scalar variables, $\dot{e}_q$ and $\dot{e}_p$, denoting deviatoric and dilatoric strain rates as introduced by Aravas (1987), have to satisfy the condition

$$\dot{e}_p\frac{\partial\Phi}{\partial q}+\dot{e}_q\frac{\partial\Phi}{\partial p}=0, \tag{6}$$

which derives from eliminating the plastic multiplier, $\dot{\lambda}$.

Finally, evolution equations for the internal variables of isotropic and kinematic hardening,

$$\left.\begin{aligned}\dot{h}^{(\alpha)}&=g(\varepsilon^{\mathrm{pl}}_{ij},s_{ij},h^{(\alpha)})\\ \overset{\nabla}{x}_{ij}&=F_{ij}(\varepsilon^{\mathrm{pl}}_{ij},s_{ij},h^{(\alpha)})\end{aligned}\right\} \tag{7}$$

complete the constitutive relations. Strain hardening materials contain a single scalar hardening variable, the accumulated equivalent plastic strain,

$$\varepsilon^{\mathrm{pl}}_{\mathrm{eq}}=\int_0^t\sqrt{2/3d^{\mathrm{pl}}_{ij}d^{\mathrm{pl}}_{ij}}\,\mathrm{d}\tau, \tag{8}$$

determining the current flow stress by a material dependent relation $R(\varepsilon^{\mathrm{pl}}_{\mathrm{eq}})$.

3. Micromechnical models

3.1. Unit cell approach

The micromechanical process of damage in a ductile material can be studied on representative volume elements (RVE) or "unit cells", in which a cavity is introduced in order to simulate a reduction of net resisting area. In this way, the microstructure of a damaged material is represented by a periodic array of cavities in an elasto-plastic ductile matrix. These cell model calculations have been used to simulate and study the behavior of porous solids in order to determine a macroscopic yield surface in the case of small overall strains (Zohdi et al., 2002) or to calibrate model parameters of continuum models which account for any kind of damage in the finite strain regime. They have mostly been used for monotonous loadings, see Koplik and Needleman (1988), Brocks et al. (1995) and Leblond et al. (1995). Investigations of unit cells under reversed loadings have been performed by Ristinmaa (1997), Devaux et al. (1997) and Besson and Guillemer-Neel (2003). Usually, the simplest configuration is chosen, that is hexagonal cylindrical cells, which are then approximated by circular cylinders to allow for simple axisymmetric calculations. They give a lower-bound limit-load solution as shown in Kuna and Sun (1996). The cell of initial diameter, L_0, and height, L_0 contains a spherical hole of radius r_0 and is subject to homogeneous radial and axial displacements. The boundaries of the cell are constrained to be straight and orthogonal. The "mesoscopic" principal strains, E_i $(i = 1, 2, 3)$, are given by

$$\left.\begin{aligned} E_1 &= E_2 = \ln\left(1 + \tfrac{\bar{u}_2}{r_0}\right) \\ E_3 &= \ln\left(1 + \tfrac{\bar{u}_3}{r_0}\right) \end{aligned}\right\}. \tag{9}$$

The correspondent "mesoscopic" true principal stresses, $\Sigma_1 = \Sigma_2$, Σ_3, are the average reaction forces at the cell boundaries per momentary areas. Here and in the following, capital letters denote quantities on a "mesoscopic" length scale and small letters quantities on a "microscopic" scale, respectively. Uniaxial equivalent stress, Σ_{eq}, and strain, E_{eq}, are defined for cyclic processes by

$$\left.\begin{aligned} \Sigma_{\mathrm{eq}} &= \Sigma_3 - \Sigma_1 \\ E_{\mathrm{eq}} &= \tfrac{2}{3}|E_3 - E_1| \end{aligned}\right\}. \tag{10}$$

Stress triaxiality is defined as the ratio of hydrostatic and von Mises equivalent stress

$$T = \frac{\Sigma_m}{\Sigma_{\mathrm{eq}}} = \frac{2\Sigma_1 + \Sigma_3}{3|\Sigma_3 - \Sigma_1|}. \tag{11}$$

The void volume fraction, f, is defined as the ratio of the current void volume, V_{void}, and the total cylinder volume, $V_{\mathrm{cyl}} = \frac{\pi}{4}L^3$. The former can be computed either via the condition of incompressibility for plastic deformations (Koplik and Needleman, 1988) or from the sum of the Jacobians of all finite elements, which equals $(V_{\mathrm{cyl}} - V_{\mathrm{void}})$.

3.2. Porous plasticity models

The damage models are formulated in the framework of the theory of rate-independent, but pressure-dependent plasticity. Models of ductile damage include (at least) one additional internal variable—besides the accumulated equivalent plastic strain, $\varepsilon_{\mathrm{eq}}^{\mathrm{pl}}$, for isotropic and back stresses, x_{ij}, for kinematic hardening—which is identical to or depends on the void volume fraction, f. The latter is defined as the ratio of the volume of all cavities in a material element to its total volume, which corresponds to the definition given for

the unit cell approach. An evolution equation holds for the void volume fraction, consisting of a void growth and a void nucleation part, in general,

$$\dot{f} = \dot{f}_{\text{growth}} + \dot{f}_{\text{nucl}} \quad \text{with } f(t_0) = f_0. \tag{12}$$

The growth term is obtained from the conservation of mass,

$$\dot{f}_{\text{growth}} = (1-f)d^{\text{pl}}_{kk}, \tag{13}$$

and the nucleation term is commonly adopted from an empirical approach by Chu and Needleman (1980) assuming a normal distribution of void nucleating particles.

The various models proposed in this context differ by the yield function, Eq. (1), mainly. The yield function of the so-called GTN model,

$$\Phi = \frac{3\sigma'_{ij}\sigma'_{ij}}{2(R(\varepsilon^{\text{pl}}_{\text{eq}}))^2} + 2q_1 f^* \cosh\left(q_2 \frac{\sigma_{kk}}{2R(\varepsilon^{\text{pl}}_{\text{eq}})}\right) - (1 + q_3 f^{*2}) = 0, \tag{14}$$

has originally been derived from micromechanical considerations by Gurson (1977). The modifications by Needleman and Tvergaard (1984); Tvergaard and Needleman (1984) concern the introduction of three additional material parameters, q_i $(i = 1,2,3)$, affecting the yield behavior and the damage variable, f^*, which equals the void volume fraction, f, up to a critical value, f_c, for beginning coalescence of voids, beyond which damage is accelerated by a factor $\kappa > 1$,

$$f^* = \begin{cases} f & \text{for } f \leqslant f_c, \\ f_c + \kappa(f - f_c) & \text{for } f > f_c. \end{cases} \tag{15}$$

The GTN model in its original form accounts for isotropic hardening, only, which limits its application to monotonous loading, in principle. Leblond et al. (1995) have extended Gurson's yield function to kinematic hardening by replacing the Cauchy stress tensor by the difference of Cauchy stress and backstress tensor, see Eq. (2), which leads to the yield function

$$\Phi = \frac{3s'_{ij}s'_{ij}}{2\bar{\sigma}_1^2} + 2f^* \cosh\left(q_2 \frac{s_{kk}}{2\bar{\sigma}_2}\right) - (1 + q_3 f^{*2}) = 0. \tag{16}$$

The quantities $\bar{\sigma}_1$, $\bar{\sigma}_2$ result from a re-calculation of the homogenisation problem for hardening material. The numerical implementation used here is described in Mühlich and Brocks (2003). Both models, the GTN and the LPD model, have been implemented as user-supplied material routines (UMAT) in the FE code ABAQUS.

3.3. CDM model

In Bonora (1997) a nonlinear damage model in the framework of continuum damage mechanics is proposed. Features of this model are:

- No softening effect appears explicitly in the material yield function. This is motivated by the fact that it is experimentally not possible to separate the hardening effect due to plastic deformation from the softening effect induced by damage evolution. Consequently, the material yield function is written:

$$\Phi(s_{ij}, R, x_{ij}) = q - f(R, x_{ij}, D) = 0, \tag{17}$$

where $f(R, x_{ij}, D)$ is the experimentally determined material flow curve where damage effects on R and x_{ij} are already taken into account.
- The damage potential is nonlinear in the accumulated plastic strain.

The CDM definition does not make any distinction between the possible way in which damage occurs from the physical standpoint. Besides, from the thermodynamics standpoint damage can only increase since the related dissipation must always be null or positive. Anyway, although the damage mechanisms and their related effects onto the overall mechanical properties are not yet established in detail in the case of cyclic plastic loading, it is generally recognized that its effects and rate of accumulation can be generally different under tension and compression, respectively (Lemaitre, 1985). To account for this fact, Pirondi and Bonora (2003) extended the formulation to the case of cyclic plastic loading according to the following hypotheses, based on the sign of the (continuum) triaxiality factor $T = \sigma_m/\sigma_{eq}$ where $\sigma_m = \frac{1}{3}\sigma_{kk}$ and $\sigma_{eq} = \sqrt{\frac{3}{2}\sigma'_{ij}\sigma'_{ij}}$:

- Damage accumulates and its effect on material stiffness is active if and only if T is positive, i.e.

$$\text{if} \quad \sigma_m/\sigma_{eq} \geqslant 0 \quad \text{and} \quad \varepsilon \geqslant \varepsilon_{th} \mapsto \dot{D} > 0, \quad D \neq 0 \quad \text{and} \quad E = E_0(1-D). \tag{18}$$

- Damage does not accumulate and its effects are inactive if T is negative,

$$\text{if} \quad \sigma_m/\sigma_{eq} < 0 \quad \text{and} \quad D > 0 \mapsto \dot{D} = 0 \quad \text{and} \quad E = E_0. \tag{19}$$

The complete set of constitutive equation can be written as follows:

$$\varepsilon_{ij}^{el} = \frac{1+\nu}{E}\frac{\sigma_{ij}}{1-D} - \frac{\nu}{E}\frac{\sigma_{kk}}{1-D}\delta_{ij}, \tag{20}$$

$$d_{ij}^{pl} = \dot{\lambda}\frac{\partial \Phi}{\partial \sigma_{ij}} = \frac{3}{2}\dot{\lambda}\frac{s'_{ij}}{s_{eq}}, \tag{21}$$

$$\dot{x}_{ij} = -\dot{\lambda}\frac{\partial \Phi}{\partial x'_{ij}} = d_{ij}^{pl} - \frac{3}{2X_\infty}x'_{ij}\dot{\lambda}, \tag{22}$$

$$\dot{h} = -\dot{\lambda}\frac{\partial \Phi}{\partial R} = \dot{\lambda} = d_{ij}^{pl}, \tag{23}$$

$$\dot{D}^{+} = \alpha \cdot \frac{(D_{cr}-D_0)^{1/\alpha}}{\ln(\varepsilon_f/\varepsilon_{th})} \cdot f\left(\frac{\sigma_m}{\sigma_{eq}}\right) \cdot (D_{cr}-D^{+})^{\frac{\alpha-1}{\alpha}} \cdot \frac{\dot{\varepsilon}_{eq}^{pl+}}{\varepsilon_{eq}^{pl+}}, \tag{24}$$

$$\dot{\varepsilon}_{eq}^{pl+} = \dot{\lambda} \cdot H\langle f(\sigma_m/\sigma_{eq})\rangle, \tag{25}$$

$$E = E_0\left(1 - D^{+}H\langle f(\sigma_m/\sigma_{eq})\rangle\right), \tag{26}$$

where

$$H\langle f(\sigma_m/\sigma_{eq})\rangle = \begin{cases} 0 & \sigma_m/\sigma_{eq} < 0, \\ 1 & \sigma_m/\sigma_{eq} \geqslant 0. \end{cases} \tag{27}$$

The superscript "+" indicates quantities increasing only if triaxiality is positive.

4. Modelling

4.1. Material

The material considered in this work is a German low alloy steel 20MnNiMo55 (similar to A508 in the US designation). In Tables 1 and 2 respectively, the reference composition and the standard mechanical

Table 1
Chemical composition of 20MnMoNi55 steel

C	Si	Mn	P	S	Cr	Mo	Ni
0.19	0.2	1.29	0.007	0.008	0.12	0.53	0.8

Table 2
Standard mechanical properties of 20MnMoNi55 steel

Upper yield strength (MPa)	Tensile strength (MPa)	Elongation at failure (%)	Contraction at failure (%)
481	581	25.6	67.6

properties are given. Its cyclic hardening behavior is described with the model of Chaboche (1989), which combines a nonlinear kinematic and isotropic hardening. An analytical relation with an initial yield stress, R_0, and a saturation value, R_∞, is applied for the isotropic flow stress,

$$R = R_0 + (R_\infty - R_0)(1 - \mathrm{e}^{-b\varepsilon_{\mathrm{eq}}^{\mathrm{pl}}}), \tag{28}$$

and an extension of Ziegler's law with an additional recall-term for the evolution of back stresses

$$\dot{x}_{ij} = \frac{C}{R(\varepsilon_{\mathrm{eq}}^{\mathrm{pl}})} s_{ij} \dot{\varepsilon}_{\mathrm{eq}}^{\mathrm{pl}} - \gamma x_{ij} \dot{\varepsilon}_{\mathrm{eq}}^{\mathrm{pl}}. \tag{29}$$

This model allows to reproduce most of the features of the cyclic plastic behavior such as Bauschinger effect, cyclic hardening or softening, ratchetting of strain under constant stress amplitude and relaxation of mean stress. The model parameters, namely R_0, R_∞, b, C, γ, have been inferred from the first 10 loading cycles of cyclic loading tests made on round bars of 20MnMoNi55 steel, since the comparison of the performance of the different models is made within this number of cycles. In this interval, the material showed strain hardening behavior, therefore the parameters were tuned on this basis as $R_0 = 396.6$ MPa, $R_\infty = 471.6$ MPa, $b = 8$, $C = 7500$ MPa, $\gamma = 70$.

Model parameters used for the porous metal plasticity models were taken either from quantitative microstructural analysis or from the literature Bernauer and Brocks (2002). The initial void volume fraction in the unit cell approach, the GTN- and LPD models was set to 0.001. The values of q_1, q_2 and q_3 are 1.5, 1.0 and 2.25, respectively. In this study the coalescence of voids subjected to cyclic deformation is not considered. Therefore, in the simulations, the parameter κ was set equal to 1, which leads to $f^* = f$ for all times. As the investigation should cover solely the void growth mechanism, void nucleation Chu and Needleman (1980) is not considered here. The parameters of the CDM model α, D_{cr}, D_0, ε_f, $\varepsilon_{\mathrm{th}}$ employed here were evaluated by fitting the results of tests in which the damage was evaluated from the decrease of stiffness, i.e. $D = 1 - E/E_0$ and plotted as a function of plastic strain (Gentile and Pirondi, 2003). Damage in this material accumulates very steeply in the early deformation stage, almost showing a stepwise after yielding. This behavior can be connected to the presence of weakly bonded MnS inclusions (Decamp et al., 1997). A good fit of damage vs. strain just after yielding was obtained taking an initial damage $D_0 = 0.15$. The parameters of all of the models are summarized in Table 3.

4.2. FE models

For the unit cell calculations, an axisymmetric FE model representing one quarter of the cell as shown in Fig. 1 is considered. Symmetry conditions are imposed at $x_2 = 0$, $x_3 = 0$ in order to model only one quarter of the cell. Eight-noded, reduced integration elements were used. The deformation of the cell boundaries is homogeneous with help of constraint equations (''plane-remains-plane''). The radius of the spherical void

Table 3
Hardening and damage parameters of the GTN/LPD and CDM models

Hardening	R_0 (Mpa)	R_∞ (MPa)	b	C (MPa)	γ
	396.6	471.6	8	7500	70
GTN/LPD	q_1	q_2	q_3	f_0	κ
	1.5	1.0	2.25	0.001	1
CDM	D_0	D_{cr}	ε_{th}	ε_f	α
	0.15	1	0.0213	1.5	0.362

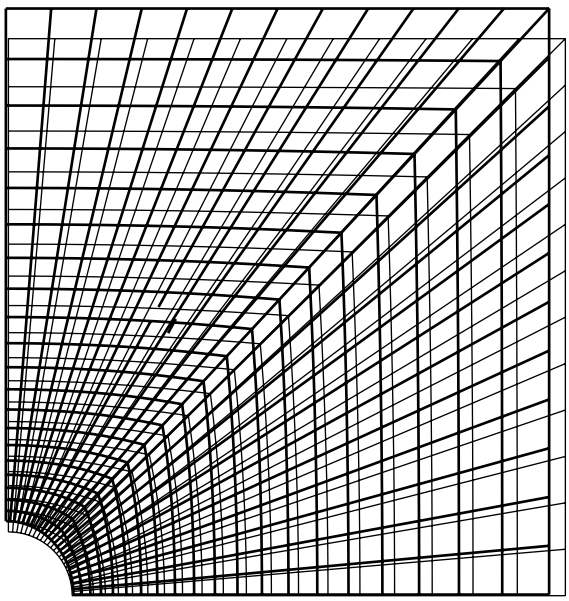

Fig. 1. Undeformed and deformed FE mesh (quarter model) of a unit cell containing a void with $f_0 = 0.001$.

was chosen in order to simulate an initial void volume fraction $f_0 = 0.001$. The cell is subjected to radial and axial stresses following a prescribed history, $\Sigma_2(t)$, $\Sigma_3(t)$. In order to have constant mesoscopic triaxiality, Eq. (11), during the entire load cycle, the ratio of Σ_3/Σ_2 has to be kept constant. If the simulation is run with constant strain amplitudes, the current value of the equivalent stress has to be checked in every time step and the applied stress controlled as necessary. Simulations were performed with a triaxiality factor $T = 1/3$ (uniaxial state of stress), $T = 1$ (intermediate constraint) and $T = 2$ (severe constraint), respectively. The range of the equivalent strain, E_{eq} , was chosen to be 0.03 or 0.05, respectively. The strain ratio was chosen to be $R_\varepsilon = 0$ (positive strains) and $R_\varepsilon = -1$ (symmetric cycle). The same approach has been followed for the simulation with the LPD and CDM models, except that in this case the mesh is made of a single element.

5. Results and discussion

Fig. 2 shows the overall (or mesoscopic) equivalent stress–strain curve of a unit cell for $T = 1$ under repetitive strain, $E_{eq} = 0.05$, $R_\varepsilon = 0$, for purely isotropic and purely kinematic hardening. The respective

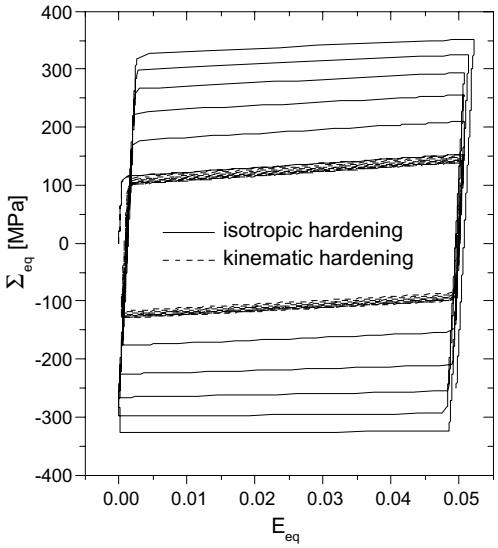

Fig. 2. Cyclic overall (mesoscopic) equivalent stress–strain curve of a unit cell under $T = 1$ for pure isotropic and pure kinematic hardening.

material parameters for this particular numerical study have been determined in order to show an identical stress–strain curve during the first cycle and are therefore not related to the steel 20MnNiMo55 envisaged above. Moreover, the model parameters are chosen in a way that the isotropic hardening does not saturate in the considered strain range. Thus, hardening parameters $R_0 = 115$ MPa, $C = 700$ MPa and $\gamma = 2$ were used to describe the kinematic hardening. The respective yield function for pure isotropic hardening was then defined by data points. For the cell with isotropic hardening, the mesoscopic stress is increasing with the number of cycles. In the case of kinematic hardening, a slight shift of the stress response is observed, which cannot be explained by means of the hardening model, only. As the stress field in the cell depends on the hardening model chosen, this will affect the evolution of the void volume fraction of the cell and thus influence the mesoscopic stress response.

More interesting, however, is the evolution of the void volume and the question whether it is reversible or increases with increasing number of load cycles. The latter will be addressed as ''ratchetting'' and is a necessary condition for accumulation of damage on the microscopic level leading to final failure. Fig. 3 shows the normalised void volume fraction, f/f_0, in dependence on the equivalent overall strain, E_{eq}, for the same numerical test depicted in Fig. 2. Note, that both cyclic curves start at $f/f_0 = 1$. The unit cell with isotropic hardening material shows an increasing void volume fraction after the first cycle, followed by a stabilisation. The prediction based on pure kinematic hardening is rather complex, starting with $f/f_0 < 1$ after the first cycle at $E_{\mathrm{eq}} = 0$ and subsequently increasing void volume fraction in the following cycles. An analogous simulation with ideal plastic behavior of the matrix material (not shown here) does not show any ratchetting of the void volume fraction at all.

In the following, the hardening behavior as well as the damage model parameters described in Section 4 are used, see Table 3. The mesoscopic behavior of the unit cell and the performance of the two damage models, namely the LPD and the CDM model, is displayed in Figs. 4–6 for different triaxialities. In this investigation, a symmetric loading cycle ($R_\varepsilon = -1$) is prescribed. For the sake of easier understanding, the absolute value in the definition of the mesoscopic equivalent strain, Eq. (10), was dropped. In this case, E_{eq} can reach negative values. The relative void volume fraction, f/f_0, is plotted as a function of the mesoscopic strain difference, $E_3 - E_1$, for the unit cell models and as a function of the microscopic strain

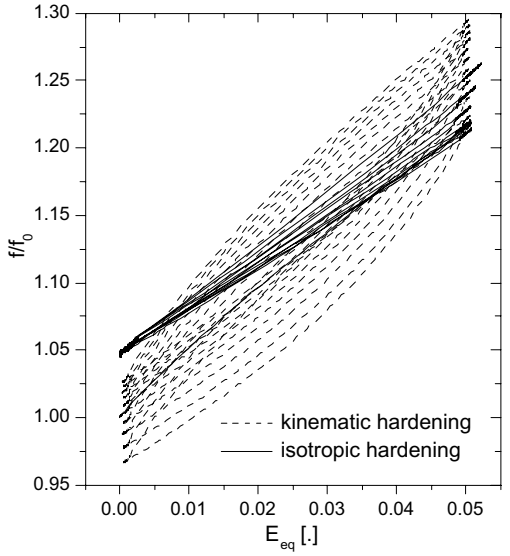

Fig. 3. Response of a unit cell: void volume fraction vs. equivalent strain; pure isotropic and pure kinematic hardening, $T = 1$.

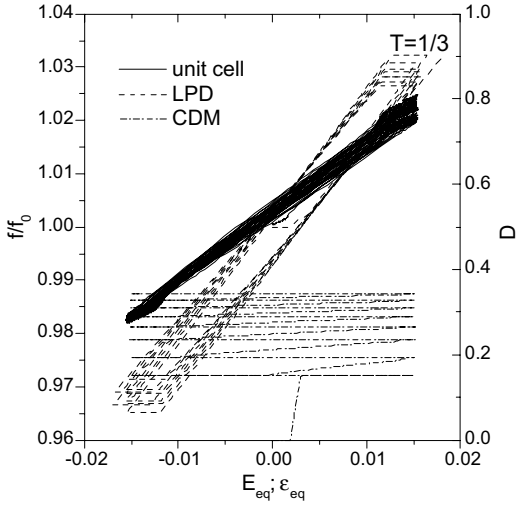

Fig. 4. Response of a unit cell and single element for LPD and CDM models: void volume fraction vs. equivalent strain; combined hardening, $T = 1/3$ (parameter see Table 3).

difference, $\varepsilon_3 - \varepsilon_1$, for the LPD and CDM models. The assumption of a unit cell as a representative volume element allows for the comparison of the "internal variables" as a function of the effective kinematic quantities.

For the LPD model, porosity remains constant during elastic unloading. This effect is due to the fact that void evolution is triggered by the plastic strain rate, see Eq. (13). On the other hand, the evolution of void volume fraction in the case of the unit cell allows for a decrease during unloading. More interesting, however, is that for all triaxialities a ratchetting of the void volume fraction is observed in the case of the unit

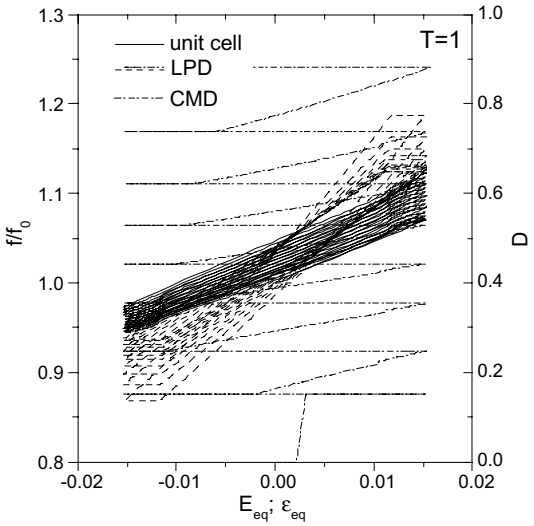

Fig. 5. Response of a unit cell and single element for LPD and CDM models: void volume fraction vs. equivalent strain; combined hardening, $T = 1$ (parameter see Table 3).

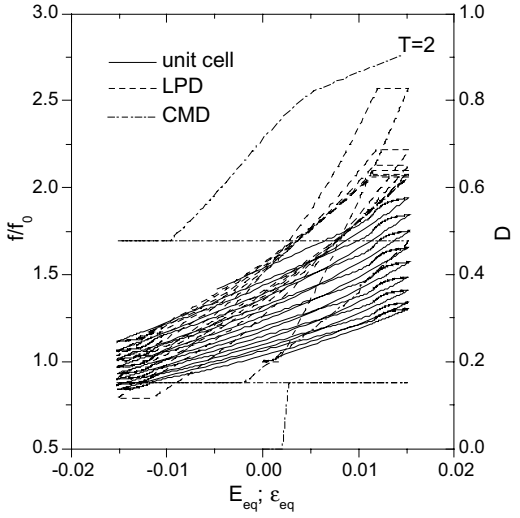

Fig. 6. Response of a unit cell an single element calculations for LPD and CDM models: void volume fraction vs. equivalent strain; combined hardening, $T = 2$ (parameter see Table 3).

cell. It appears to be very weak in the case of uniaxial tension, but is rather strong for the higher triaxialities. Thus it can be concluded that successive void growth with the number of loading cycles is a "micromechanism" of a voided material.

Damage evolution for the GTN model is not shown here, since under fixed triaxiality $f(E_{\mathrm{eq}})$ is a single curve showing no ratchetting, as Leblond et al. (1995) have proven. This holds more generally for any model with a yield function of the form $\Phi(q/R(\varepsilon_{\mathrm{eq}}^{\mathrm{pl}}), p/R(\varepsilon_{\mathrm{eq}}^{\mathrm{pl}}), f)$ if $\partial\Phi/\partial q$ and $\partial\Phi/\partial p$ are even and odd,

respectively, see Devaux et al. (1997). As a consequence, ratchetting of the void volume fraction can only be achieved if the stress triaxiality is not constant (Ristinmaa, 1997).

Since unit cell and LPD model have the same underlying micromechanical approach (i.e. porosity) the evolutions of the void volume fraction are directly comparable in Figs. 4–6. The behavior of the LPD model is different from that of the cell. The amplitude of the void volume fraction is generally higher. A change in void volume fraction with the number of cycles is observed, specially for the higher triaxialities, but it primarily affects the maximum and minimum value of f. The maximum value is decreasing, while the minimum value is increasing. After a few cycles, an almost stable cycle is achieved and the predictions of the LPD model are approaching those of the unit cells. In the case of the LPD model, the evolution of f can be tuned by adjusting the parameter q_2. Results for $q_2 = 0.8$, 1.0 and 1.2, respectively, are shown in Fig. 7 in the case of a triaxiality equal to 2. The higher the value of q_2, the faster void growth occurs during each cycle. This effect is more pronounced for high triaxialities, as q_2 directly affects the influence of the triaxiality within the yield function, see Eq. (14). Anyway, the void growth appears to be overestimated with respect to the predictions of a unit cell.

The evolution of the accumulated damage, D, in the case of the CDM model, is plotted together with the results of the unit cell and of the LPD model for the sake of a qualitative comparison, since a direct relation between D and porosity can not be given. The main difference of the CDM results compared to porous metal plasticity in terms of damage evolution is its monotonic accumulation. In the tension phase, damage is evolving, whereas in the compression phase its value is kept constant. Therefore, damage is always increasing. In the simulations depicted in Figs. 4–6, D starts to evolve from zero at the onset of plasticity, $E_{eq} > 0$ and adopts the value of D_0. After the threshold strain, ε_{th}, is reached, accumulation starts at the first reversal in tension. Note the sensitivity of damage parameter evolution on the triaxiality. As the model parameters have been fitted to experimental results, the mesoscopic stress response of all three approaches is very similar.

Nonlinear kinematic hardening has to be applied in order to describe deformation under cyclic loading realistically. The constitutive equations by Chaboche provide a sound basis for modelling the plastic deformations of the undamaged material. Damage evolution can be introduced based either on micromechanical considerations as in the porous metal plasticity (or Gurson type) models or on the concept of continuum

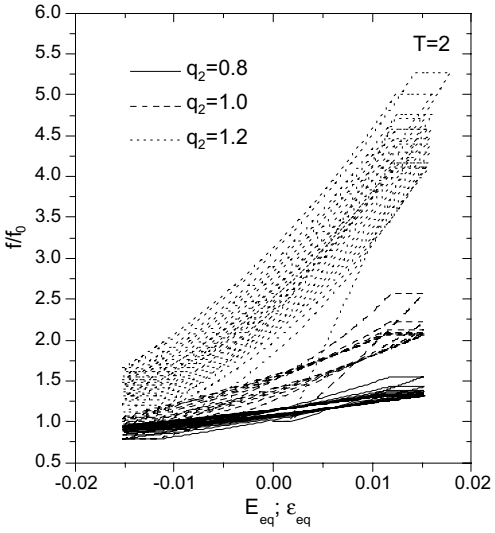

Fig. 7. Response of a single element for LPD, influence of the q_2-parameter on void volume fraction evolution, $T = 2$.

damage mechanics (CDM). If damage evolution is considered as a micromechanical process of void growth, a representative volume element (or unit cell) containing a single cavity can be considered as reference for the performance of any continuum model. Continuing void growth in every load cycle may then be regarded as a physically ensured phenomenon. Decreasing void volume under reverse loading is also observed in the unit cell which did not contain any inclusion, however. The evolution equations used in the CDM model do not regard for the phenomenon of decreasing damage, but its effect on the mechanical behavior.

Although the LPD model overestimates void growth compared to the predictions of the unit cell and the CDM model does not allow for a direct comparison of its damage parameter with the void volume fraction since it does not distinguish between voids and other kind of both models are able, however, to reproduce some qualitative features of macroscopic deformation under cyclic loading. Future investigations have to be extended to the macroscopic deformation behavior of test specimens in comparison to experimental observations.

Acknowledgments

Important contributions to this publications have been provided by S. Graff, who did his master thesis on this subject. The authors kindly acknowledge this essential input.

References

Aravas, N., 1987. On the numerical integration of a class of pressure-dependent plasticity models. Int. J. Num. Meth. Eng. 24, 1395–1416.

Aboudi, J., 1989. Micromechanical analysis of composite by the method of cells. Appl. Mech. Rev. 42 (7), 193–221.

Bernauer, G., Brocks, W., 2002. Micro-mechanical modelling of ductile damage and tearing—results of a European Numerical Round Robin. Fatigue Fract. Eng. Mater. Struct. 25, 363–384.

Besson, J., Guillemer-Neel, C., 2003. An extension of the Green and Gurson models to kinematic hardening. Mech. Mater. 35, 1–18.

Bonora, N., 1997. A nonlinear CDM model for ductile failure. Eng. Fract. Mech. 58, 11–28.

Brocks, W., Sun, D.Z., Hönig, A., 1995. Verification of the transferability of micromechanical parameters by cell model calculations with visco-plastic materials. Int. J. Plast. 11, 971–998.

Chaboche, J.L., 1989. Constitutive equations for cyclic plasticity and cyclic viscoplasticity. Int. J. Plast. 5, 247–302.

Chandrakanth, S., Pandey, P.C., 1993. A new ductile damage evolution model. Int. J. Fract. 60, R73–R76.

Chu, C.C., Needleman, A., 1980. Void nucleation effects in biaxially stretched sheets. J. Eng. Mater. Technol.—Trans. ASME 102, 249–256.

Decamp, K., Bauvineau, L., Besson, J., Pineau, A., 1997. size and geometry effects on ductile rupture of notched bars in a C–Mn steel; experiments and modelling. Int. J. Fract. 88, 1–18.

Devaux, J., Gologanu, M., Leblond, J.-B., Perrin, G., 1997. On continued void growth in ductile metals subjected to cyclic loadings. In: Willis, J.R. (Ed.), IUTAM Symposium on Nonlinear Analysis of Fracture. Kluwer Academic Publishers, Netherlands, pp. 299–310.

Gentile, D., Pirondi, A., 2003. Identificazione dei parametri di danno di un acciaio legato. In: Proc. of the XXXIIth Nat. Conf. of the Italian Association for Stress Analysis.

Gurson, A.L., 1977. Continuum theorie of ductile rupture by void nucleation and growth: Part I—Yield criteria and flow rules for porous ductile media. J. Eng. Mater. Technol.—Trans. ASME 99, 2–15.

Hughes, T.J.R., Winget, J., 1980. Finite rotation effects in numerical integration of rate constitutive equations arising in large—deformation analysis. Int. J. Num. Meth. Eng. 15, 1862–1867.

Klesnil, M., Lukas, P., 1980. Fatigue of Metallic Materials. Elsevier Science Publishers, Amsterdam.

Koplik, J., Needleman, A., 1988. Void growth and coalescence in porous plastic solids. Int. J. Solids Struct. 24, 835–853.

Kuna, M., Sun, D.Z., 1996. Three-dimensional cell model analyses of void growth in ductile materials. Int. J. Fract. 81, 235–258.

Leblond, J.-B., Perrin, G., Devaux, J., 1995. An improved Gurson-type model for hardenable ductile metals. Eur. J. Mech. A—Solids 14, 499–527.

Lemaitre, J., 1985. A continuous damage mechanics model for ductile fracture. J. Eng. Mater. Technol. 107, 83–89.

Mc Clintock, F.A., 1968. A criterion for ductile fracture by the growth of holes. J. Appl. Mech.—Trans. ASME, 363–371.
Mühlich, U., Brocks, W., 2003. On the numerical integration of a class of pressure-dependent plasticity models including kinematic hardening. Comp. Mech. 31, 479–488.
Needleman, A., Rice, J.R., 1978. Limits to ductility set by plastic flow localization. In: Koistinen, D.P. (Ed.), Mechanics of Sheet Metal Forming. Plenum Press, New York, pp. 237–267.
Needleman, A., Tvergaard, V., 1984. An analysis of ductile rupture in notched bars. J. Mech. Phys. Solids 32, 461–490.
Nemat-Nasser, S., Hori, M., 1993. Micromechanics: overall properties of heterogeneous materials. Elsevier Science Publishers, Amsterdam.
Pirondi, A., Bonora, N., 2003. Modeling ductile damage under fully reversed cycling. Comput. Mater. Sci. 26, 129–141.
Polak, J., 1991. Cyclic Plasticity and Low Cycle Fatigue Life of Metals. Elsevier Science Publishers, Amsterdam.
Rice, J.R., Tracey, D.M., 1969. On the ductile enlargement of voids in triaxial stress fields. J. Mech. Phys. Solids 17, 201–217.
Ristinmaa, M., 1997. Void growth in cyclic loaded porous plastic solid. Mech. Mater. 26, 227–245.
Rousselier, G., 1987. Ductile fracture models and their potential in local approach of fracture. Nucl. Eng. Design 105, 97–111.
Tvergaard, V., Needleman, A., 1984. Analysis of the cup-cone fracture in a round tensile bar. Acta Metall. 32, 157–169.
Zohdi, T.I., Kachanov, M., Sevostianov, I., 2002. On perfectly plastic flow in porous material. Int. J. Plast. 18, 1649–1659.